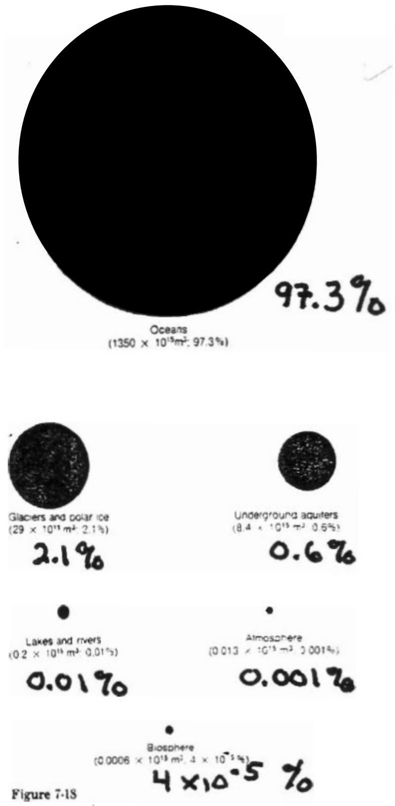

Figure 7-18

Distribution of water on the Earth. The amount of water present in various natural reservoirs is represented in terms of comparative spherical volumes. The content of each reservoir is given in cubic meters and as a percentage of the whole. Although there is an enormous quantity of groundwater, much of it may be unusable because of its high concentration of dissolved solids. [From "The Control of the Water Cycle," by J. P. Peixoto and M. Ali Kettani. Copyright © 1973 by Scientific American, Inc. All rights reserved.] Press + Siever 1986

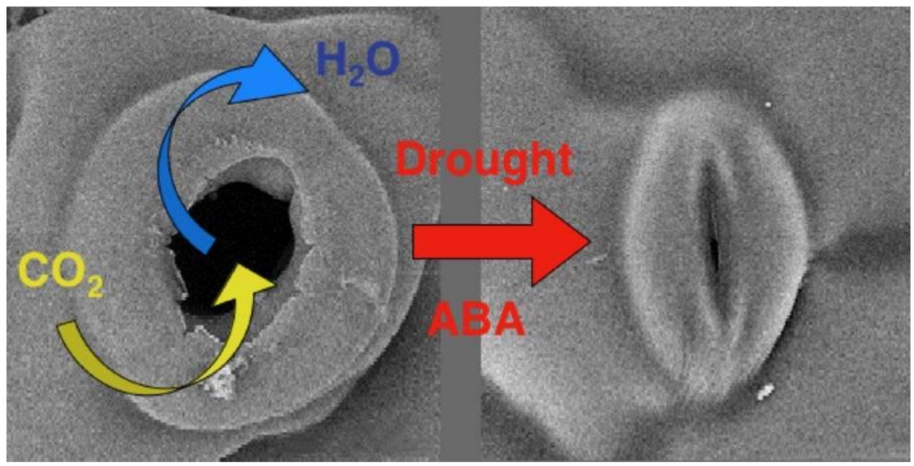

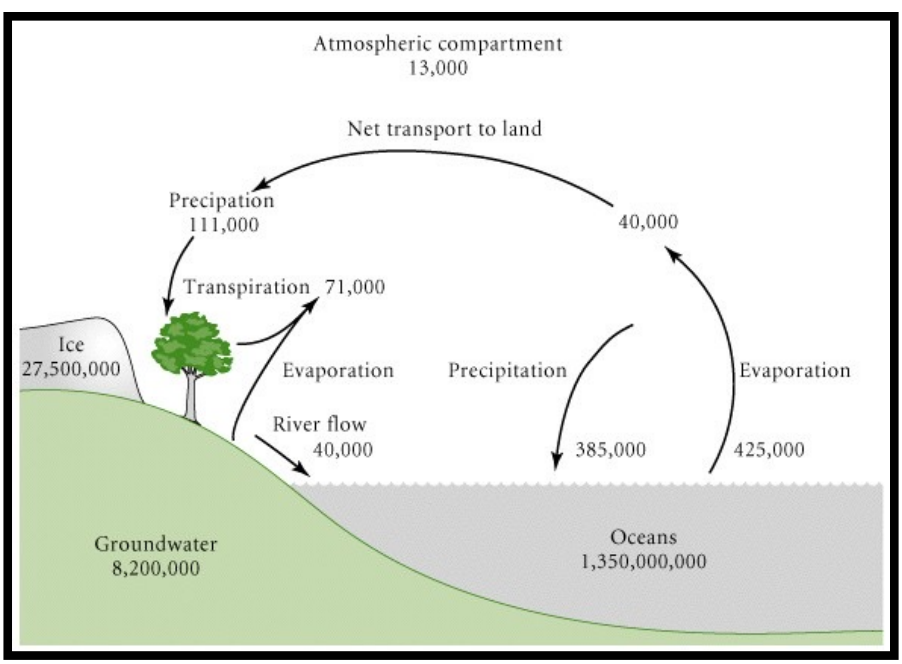

Ricklefs & Miller 2000 from Schlesinger 1991

Pools = km^3

Flows = km^3/yr

Hydrologic Cycle
(water)

Processes:

- Precipitation
- Evaporation
- Transpiration - *evaporation from leaves*
- Runoff

Fluxes

Oceans - E > P ∴ net transport of vapor to land

Land - ET < P ∴ net runoff to ocean (ca. 1/3 of P = R)

Mean Residence Time

(pg. 154 in textbook)

For a system in <u>dynamic equilibrium</u>:

<u>Mean</u> <u>Residence</u> <u>Time</u> (τ) = stock / inflow or outflow

$$\tau = 100 \text{ L} / 10 \text{ L/sec} = 10 \text{ sec}$$

τ = *Average length of time a given atom or molecule spends in the system between entering and leaving.*

What is τ for the entire ocean?

What is τ for the entire water vapor in the atmosphere?

Why do you think sulfur in WV coal that's burned upwind in Ohio, returns to WV as sulfuric acid in acid rain?

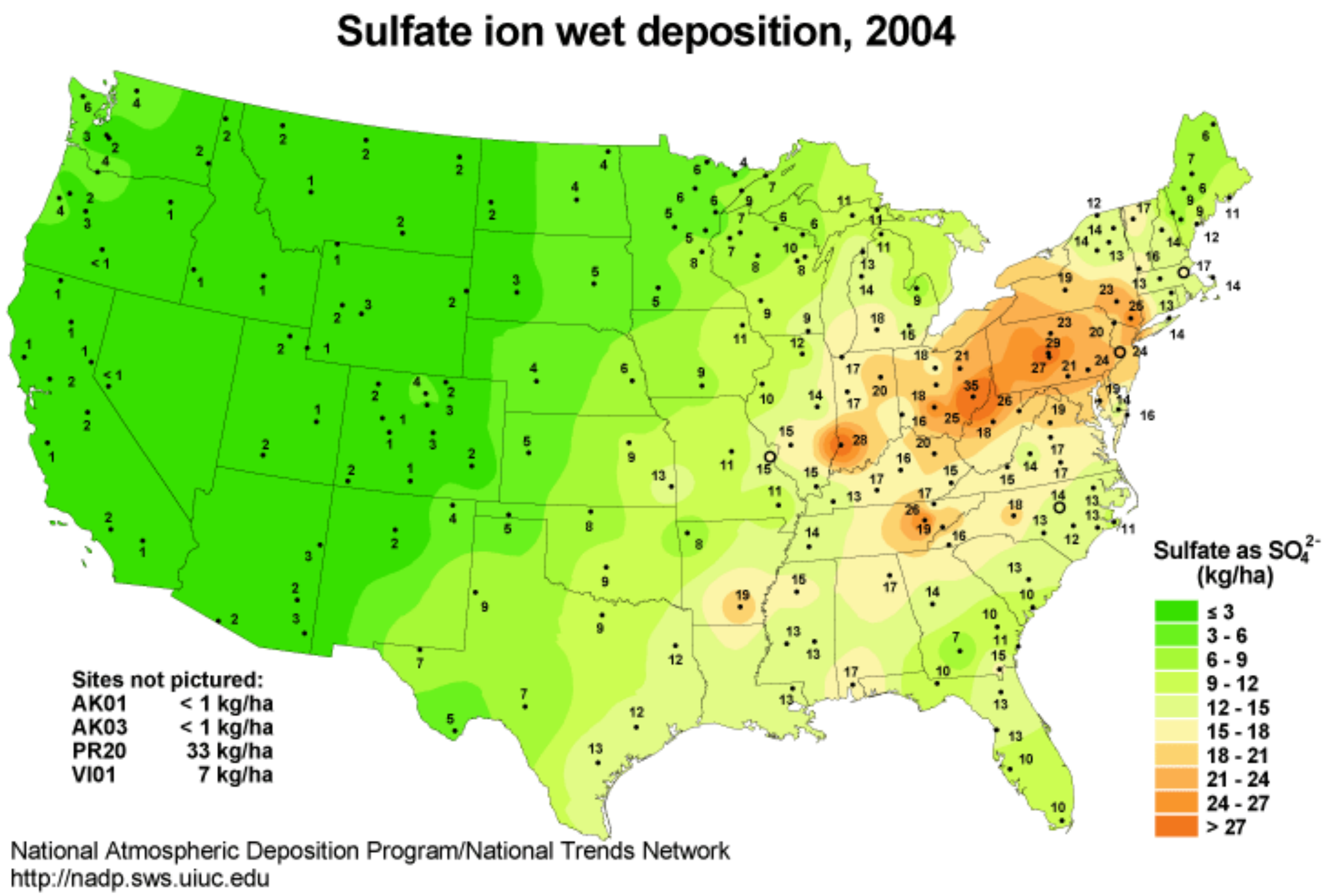

Also

τ = the **Characteristic Response Time** for a system responding to a large imbalance in inflow and outflows.
(pg. 154 textbook)

More precisely …

If removal rate is proportional to size the amount of material in the system, then the CRT is the time it takes for the amount of material in a system to decrease to ~37% of its original size when steady state is disturbed such that the outflow rate exceeds the inflow rate and the outflow depends on the amount of material in the system.

If removal rate is proportional to size the amount of material in the system, then the system behaves in a manner similar to radioactive decay.

$A_t = A_0 * e^{-kt}$ where: A = amount in system; t = time; $k = 1/\tau$

$0.37A_0 = A_0 * e^{-kt}$

$(1/e)A_0 = A_0 * e^{-kt}$ note: (1/e) = 0.37 or 37%

$e^{-1} = e^{-kt}$

$-1 = -kt$

$t = 1/k = \tau$

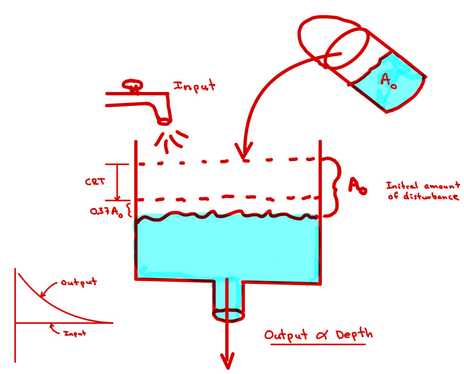

Regional Variability in the Hydrologic Cycle

E_{Ocean} ~ 4 mm/day in tropics
< 1mm/day near poles

P_{land} > 250 cm/yr Rainforests
< 25 cm/yr Deserts

Net P = (P – ET)

Highest near equator
Lowest in subtropics
P >> ET in tropical rainforests
$R_{tropics} \sim 0.5$ P
P ~ ET in deserts

Sources of P

$P_{ocean} \rightarrow E_{ocean}$

P_{land} Monsoonal climate → E_{ocean}

Amazon rainforest → ~ 0.5P from ET_{Amazon}

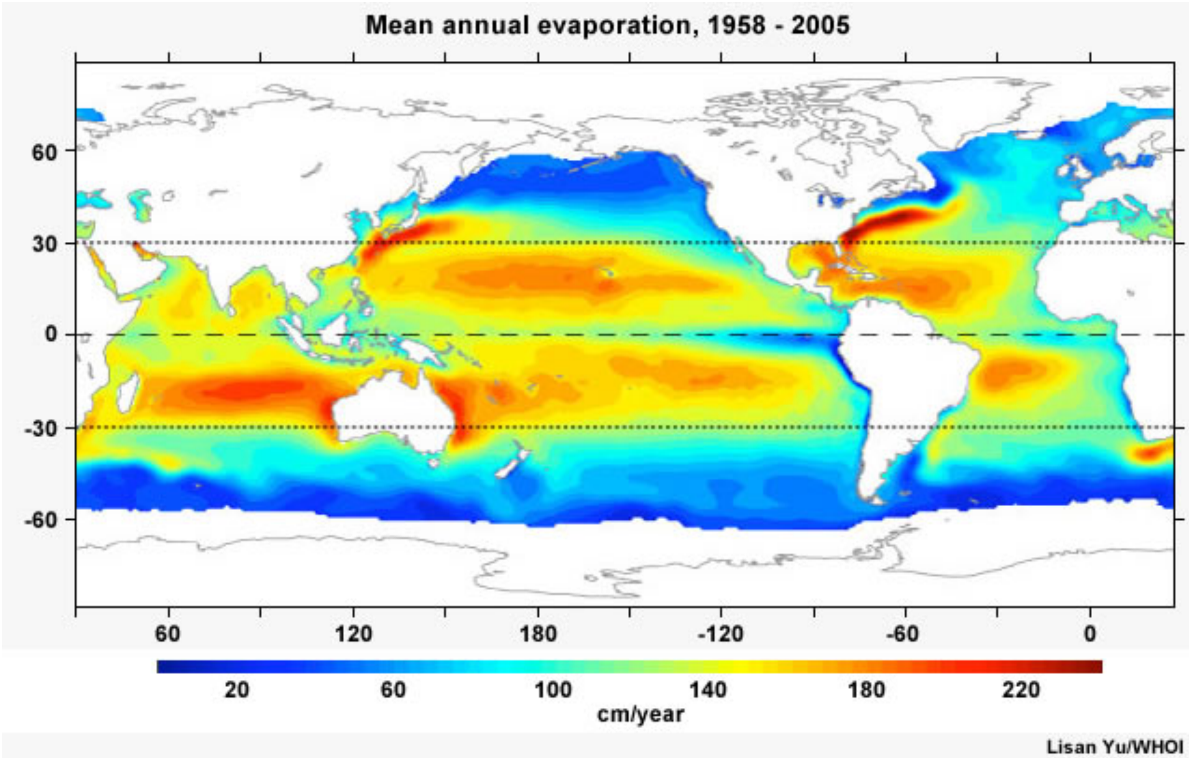

Annual total precipitation (cm, GPCP)

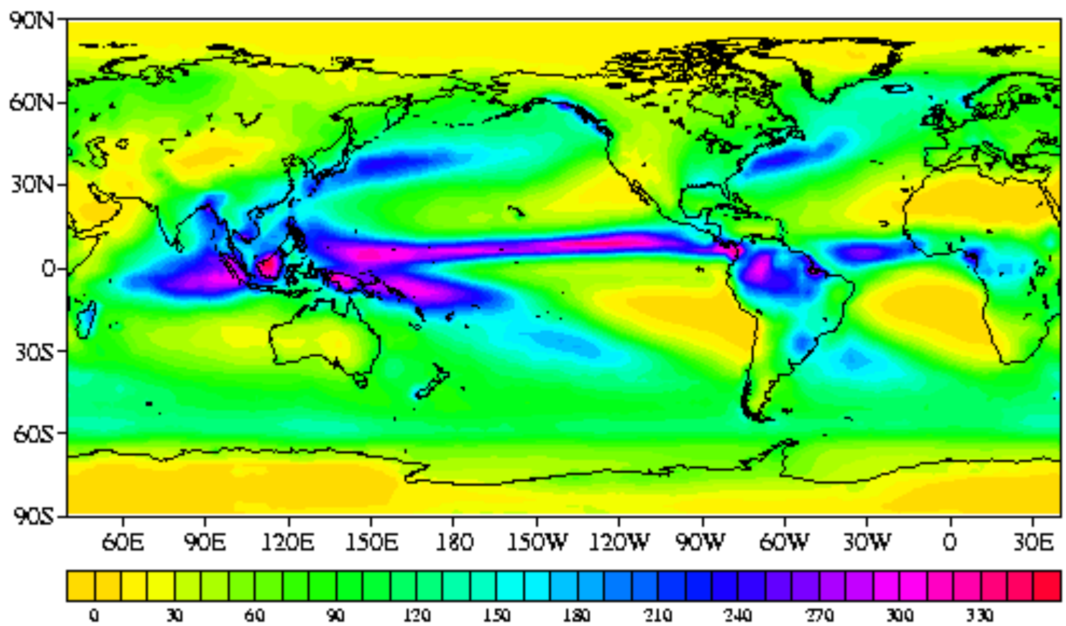

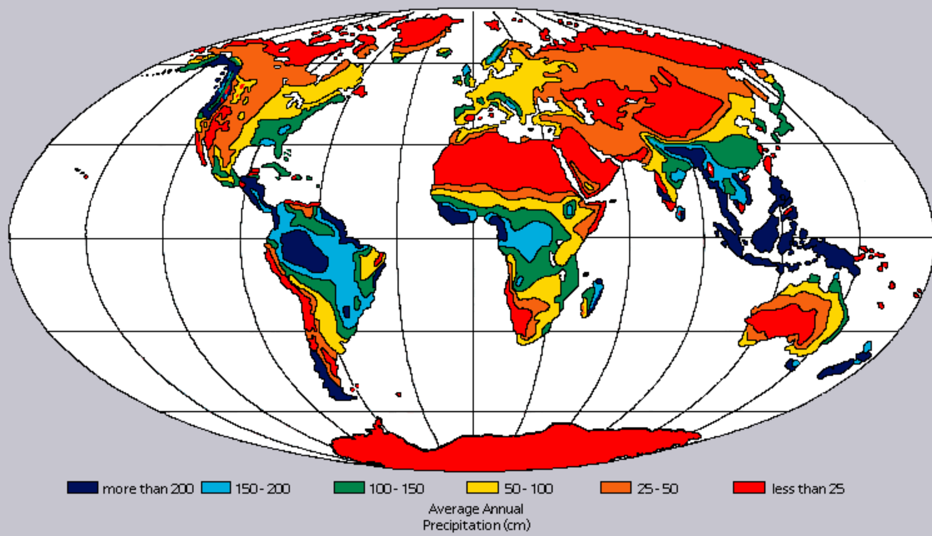

Figure 5. Global average annual precipition. (From H. L. Penman, "The Water Cycle." Copyright © September 1970 by Scientific American, Inc. All rights reserved.)

Berner, Elizabeth Kay and Robert A. Berner, 1987, *The Global Water Cycle*: Prentice-Hall, Inc., New Jersey, p. 16.

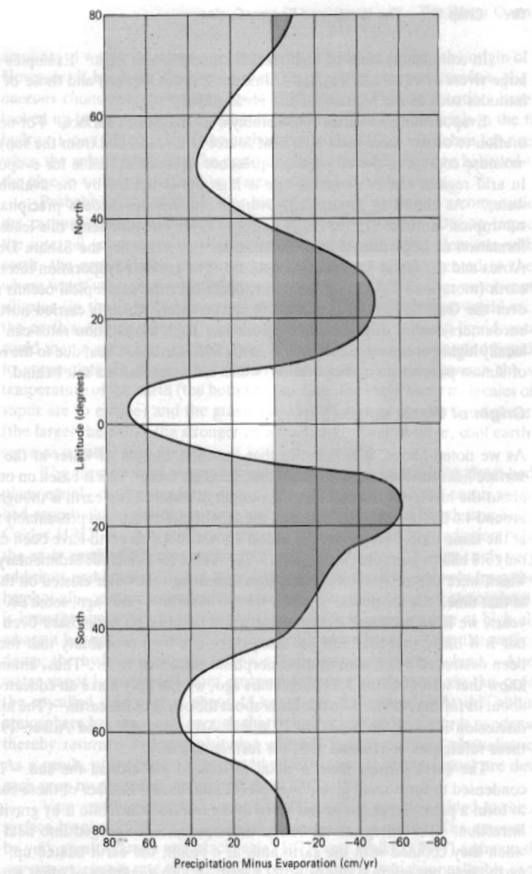

Figure 2.3 Net precipitation (precipitation minus evaporation) as a function of latitude. Positive values represent net precipitation while negative values represent net evaporation. (From J. P. Peixoto and M. A. Kettani, "The Control of the Water Cycle." Copyright © April 1973 by Scientific American, Inc. All rights reserved.)

Berner & Berner 1987

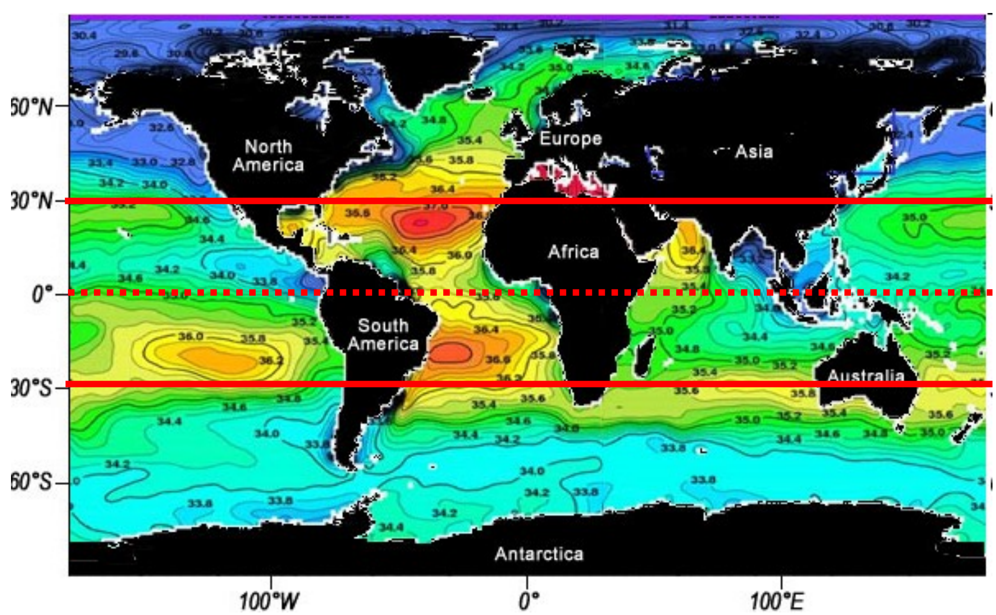

Paired Watershed Experiments

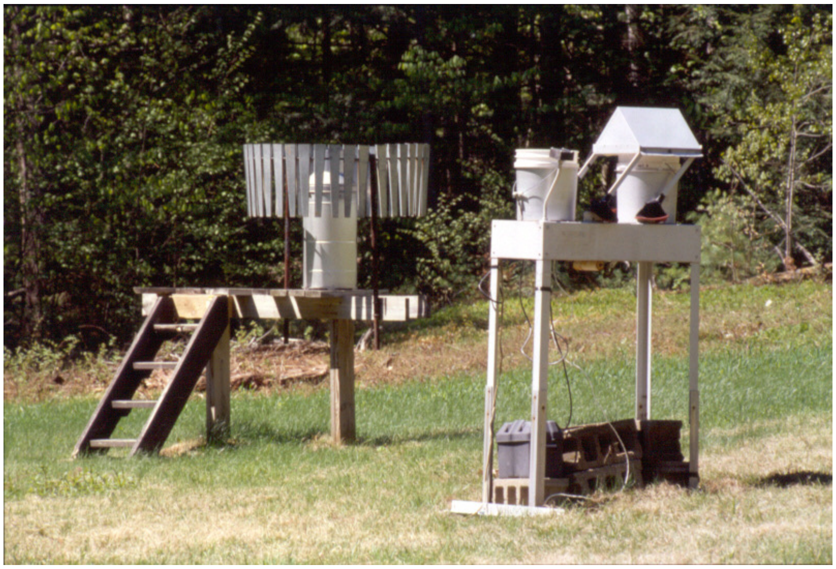

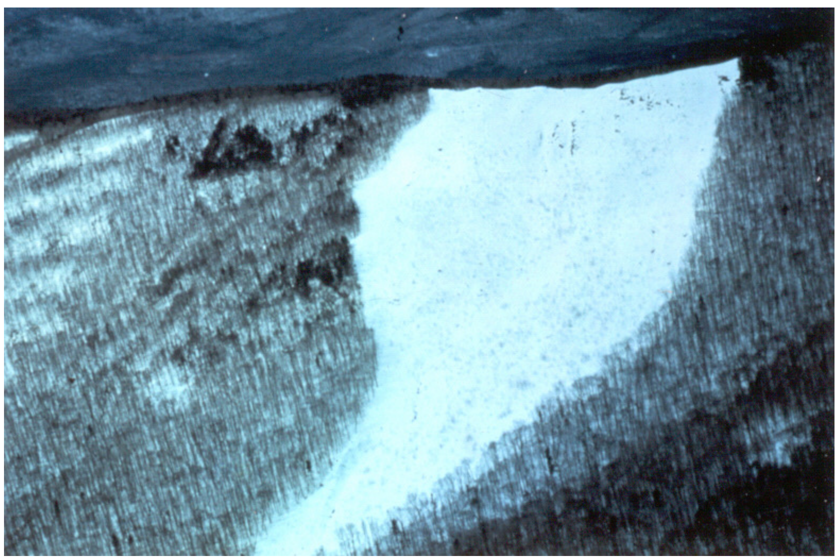

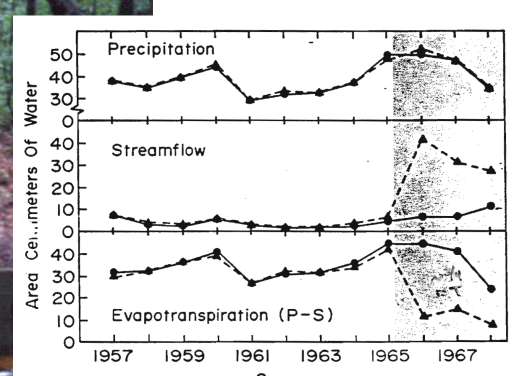

Figure 3-2. Summer hydrology, 1 June through 30 September. (●—●) Watershed 6, aggrading forest ecosystem; (▲---▲) Watershed 2, deforested during November and December of 1965 and maintained bare by herbicide treatments. Shaded area represents period when Watershed 2 was devegetated.

Bormann & Likens 1981

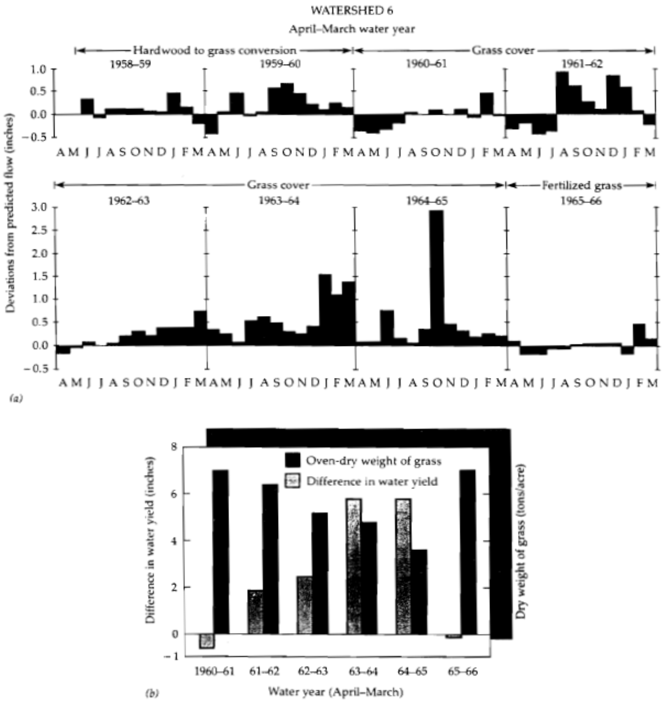

Figure 4.4
Results of forest-to-grass conversion at the Coweeta Hydrologic Laboratory. *(a)* Changes in seasonal streamflow due to conversion and the addition of fertilizer. *(b)* Relationship between increases in streamflow and the net primary production of grass. (Hibbert 1969)

Aber & Melillo 1991

Fernow Experimental Forest
Parsons, WV

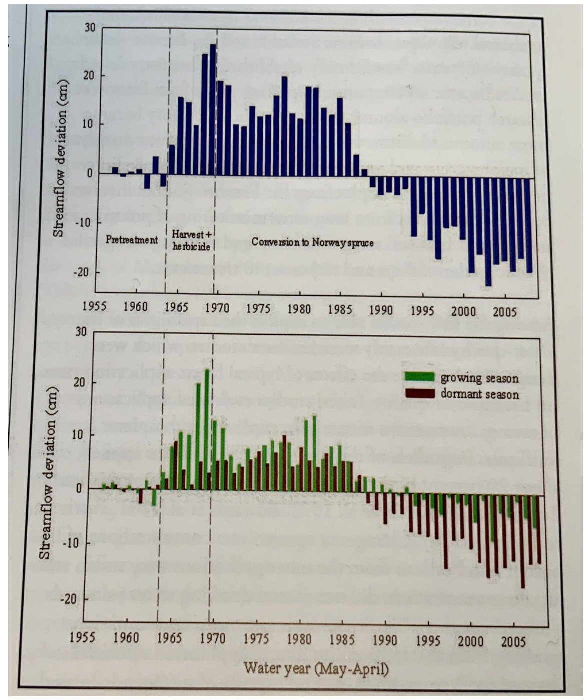

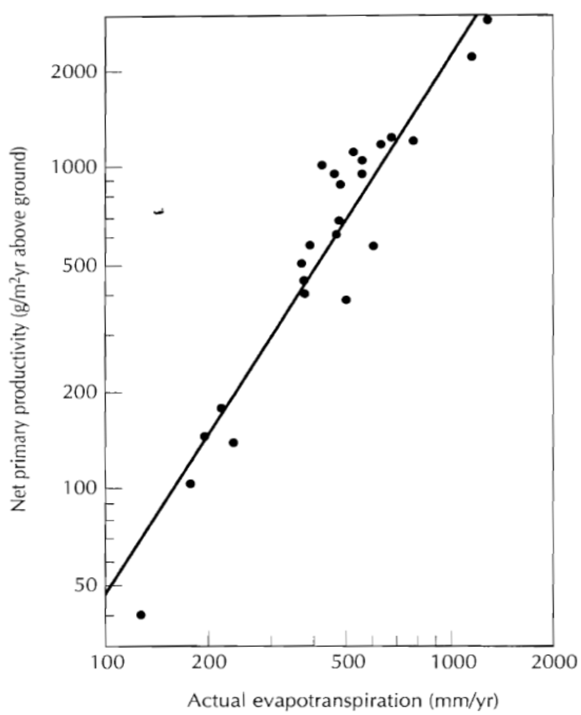

FIGURE 2.6 Net primary productivity of terrestrial ecosystems in relation to actual evapotranspiration. (Rosenzweig 1968, cited in Whittaker 1975)

Table 2. The increase or decrease in annual streamflow for four manipulated Coweeta watersheds compared to the original hardwood forests on the catchments.

Water year (May-April)	Change in streamflow (cm)			
	Grass-to-forest succession	Coppice regrowth	White pine plantations	
	Watershed 6	Watershed 13	Watershed 1	Watershed 17
1969-70	+5	+9	-18	-14
1970-71	+7	+9	-17	-10
1971-72	+5	+10	-18	-20
1972-73	+3	+5	-19	-18
1973-74	+6	+20	-18	-25
1974-75	+3	+13	-18	-24
1975-76	+3	NA	-18	-19

Swank & Douglas 1977

Recent changes in the hydrologic cycle.

========================

Streamflow has increased globally by 3% during the last
65 years

Precipitation on land has increased globally by 1% during the last 100 years.

========================

What fraction of the increased streamflow could be due to the increase in precipitation?

Since R_{ocean} = 40, 000 km^3/yr, then
R_{ocean} has increased at a rate of 1,200 km^3/65 years = 18.4 km^3/yr

Since P_{land} = 111,000 km^3/yr, then
P_{land} had increased at a rate of 1,110 km^3/100 yrs = 11 km^3/yr

Of the increased runoff to the Ocean, at most ~ 60% (11/18.4*100) can be explained by the increased amount of precipitation over land.

This would leave at least 40% of the increased due to other factors.

Vol 439|16 February 2006|doi:10.1038/nature04504 nature

LETTERS

Detection of a direct carbon dioxide effect in continental river runoff records

N. Gedney[1], P. M. Cox[2], R. A. Betts[3], O. Boucher[3], C. Huntingford[4] & P. A. Stott[5]

Continental runoff has increased through the twentieth century[1,2] despite more intensive human water consumption[3]. Possible reasons for the increase include: climate change and variability, deforestation, solar dimming[4], and direct atmospheric carbon dioxide (CO_2) effects on plant transpiration[5]. All of these mechanisms have the potential to affect precipitation and/or evaporation and thereby modify runoff. Here we use a mechanistic land-surface model[6] and optimal fingerprinting statistical techniques[7] to attribute observational runoff changes[1] into contributions due to these factors. The model successfully captures the climate-driven inter-annual runoff variability, but twentieth-century climate alone is insufficient to explain the runoff trends. Instead we find that the trends are consistent with a suppression of plant transpiration due to CO_2-induced stomatal closure. This result will affect projections of freshwater availability, and also represents the detection of a direct CO_2 effect on the functioning of the terrestrial biosphere.

Changes in climate and land use have a larger direct impact than rising CO_2 on global river runoff trends

Shilong Piao*, Pierre Friedlingstein*†, Philippe Ciais*, Nathalie de Noblet-Ducoudré*, David Labat‡, and Sönke Zaehle*

*Institut Pierre Simon Laplace, Laboratoire des Sciences du Climat et de l'Environnement, Commissariat à l'Énergie Atomique, 91191 Gif sur Yvette, France; and ‡Laboratoire de Mécanisme de Transfert en Géologie, Unité Mixte de Recherche 5563, Centre National de la Recherche Scientifique/Institut de Recherche pour le Développement/Université de Paris Sud 14, Avenue Edouard Belin, 31400 Toulouse, France

Communicated by Inez Y. Fung, University of California, Berkeley, CA, August 3, 2007 (received for review October 25, 2006)

The significant worldwide increase in observed river runoff has been tentatively attributed to the stomatal "antitranspirant" response of plants to rising atmospheric CO_2 [Gedney N, Cox PM, Betts RA, Boucher O, Huntingford C, Stott PA (2006) *Nature* 439: 835–838]. However, CO_2 also is a plant fertilizer. When allowing for the increase in foliage area that results from increasing atmospheric CO_2 levels in a global vegetation model, we find a decrease in global runoff from 1901 to 1999. This finding highlights the importance of vegetation structure feedback on the water balance of the land surface. Therefore, the elevated atmospheric CO_2 concentration does not explain the estimated increase in global runoff over the last century. In contrast, we find that changes in mean climate, as well as its variability, do contribute to the global runoff increase. Using historic land-use data, we show that land-use change plays an additional important role in controlling regional runoff values, particularly in the tropics. Land-use change has been strongest in tropical regions, and its contribution is substantially larger than that of climate change. On average, land-use change has increased global runoff by 0.08 mm/year^2 and accounts for ≈50% of the reconstructed global runoff trend over the last century. Therefore, we emphasize the importance of land-cover change in forecasting future freshwater availability and climate

PNAS 2007

Humans appropriate >50% of the accessible freshwater on Earth

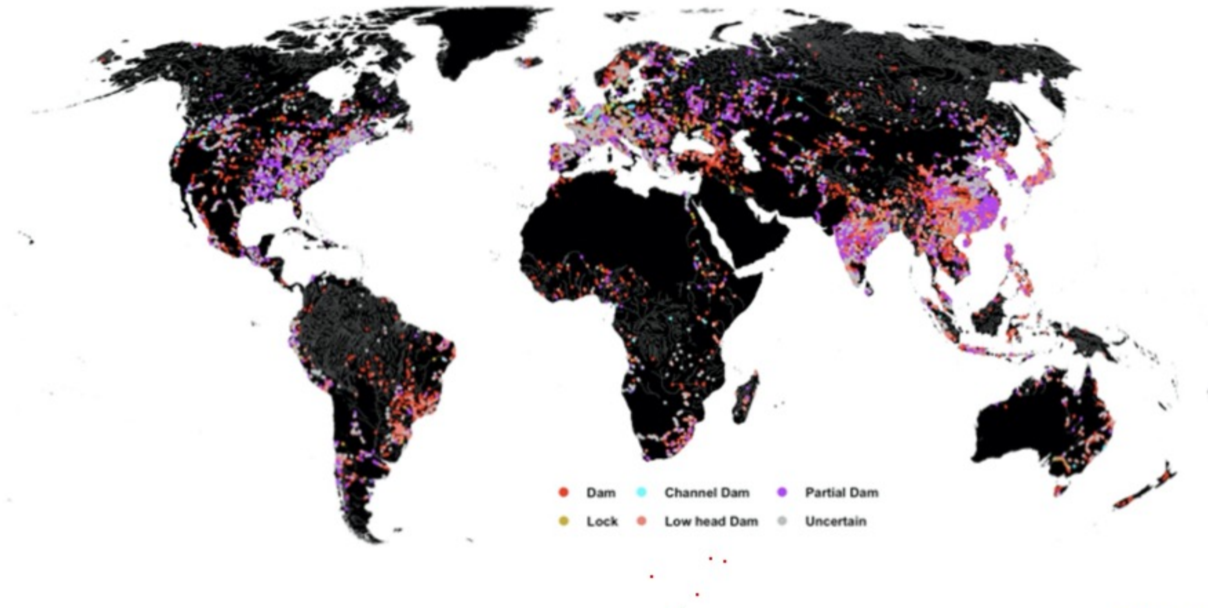

River obstructions worldwide are largely clustered in highly developed areas in North America, Europe, and South and East Asia. Credit: Global River Widths from Landsat Database and Global River Obstruction Database project members

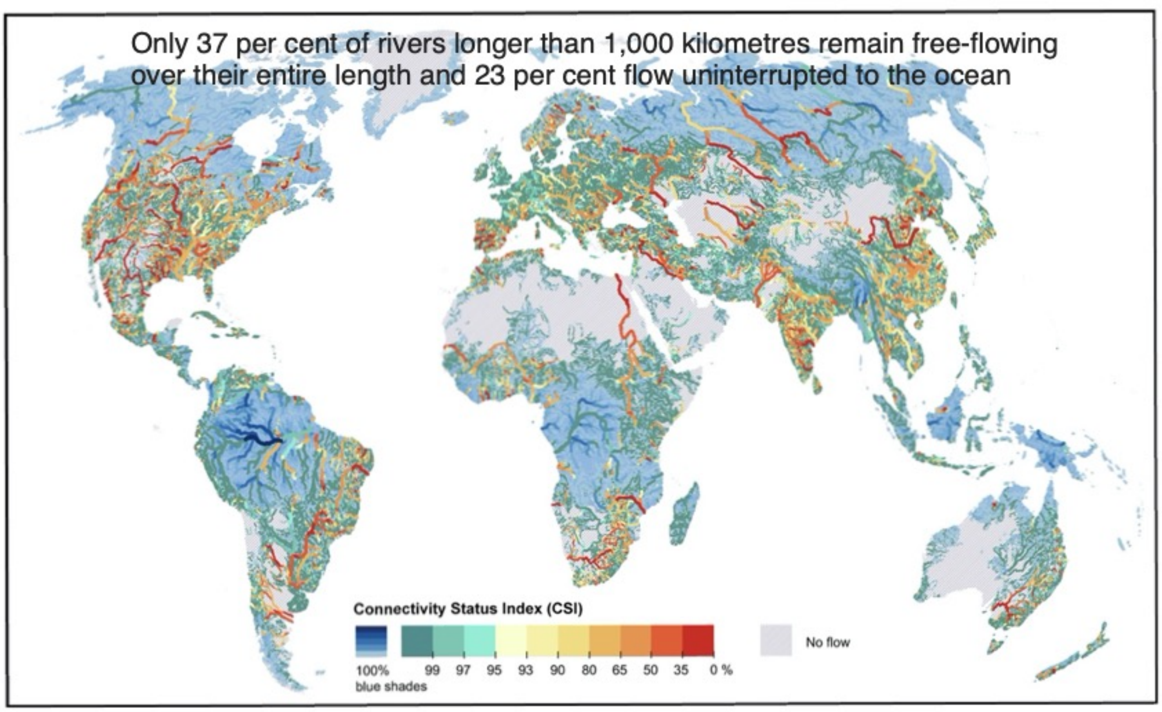

A map of global rivers' free-flowing status. Credit: Grill et al., 2019, https://doi.org/10.1038/s41586-019-1111-9

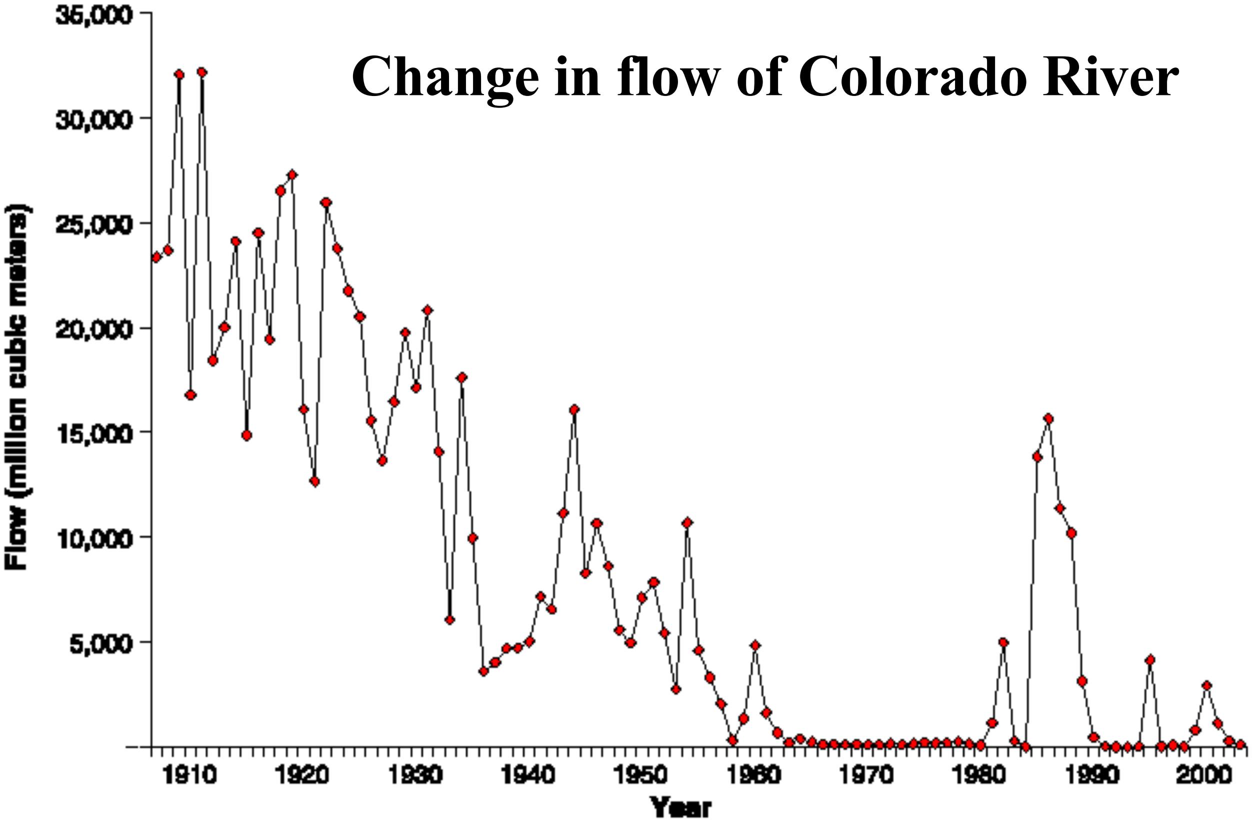

July - September, 1989

August 12, 2003

Geophysical Research Letters

RESEARCH LETTER
10.1029/2020GL088946

The Color of Rivers

John R. Gardner[1,2], Xiao Yang[1], Simon N. Topp[1], Matthew R. V. Ross[3], Elizabeth H. Altenau[1], and Tamlin M. Pavelsky[1]

[1]Department of Geological Sciences, University of North Carolina at Chapel Hill, Chapel Hill, NC, USA, [2]Department of Geology and Environmental Science, University of Pittsburgh, Pittsburgh, PA, USA, [3]Department of Ecosystem Science and Sustainability, Colorado State University, Fort Collins, CO, USA

Key Points:
- ~15.9 million satellite observations over 35 years show USA rivers (>60 m wide) are dominantly yellow and green in color
- River color has three distinct seasonal patterns that are synchronous with flow regimes
- River color significantly changed over the last three decades in one third of large US rivers

Supporting Information:
- Supporting Information S1

Correspondence:
J. R. Gardner,
gardner.john@pitt.edu

Citation:
Gardner, J. R., Yang, X., Topp, S. N., Ross, M. R.. V., Altenau, E. H., & Pavelsky, T. M. (2021). The color of rivers. *Geophysical Research Letters*, *48*, e2020GL088946. https://doi.org/10.1029/2020GL088946

Received 21 MAY 2020
Accepted 19 NOV 2020

Abstract Rivers are among the most imperiled ecosystems globally, yet we do not have broad-scale understanding of their changing ecology because most are rarely sampled. Water color, as perceived by the human eye, is an integrative measure of water quality directly observed by satellites. We examined patterns in river color between 1984 and 2018 by building a remote sensing database of surface reflectance, RiverSR, extracted from 234,727 Landsat images covering 108,000 kilometers of rivers > 60 m wide in the contiguous USA. We found 1) broad regional patterns in river color, with 56% of observations dominantly yellow and 38% dominantly green; 2) river color has three distinct seasonal patterns that were synchronous with flow regimes; 3) one third of rivers had significant color shifts over the last 35 years. RiverSR provides the first map of river color and new insights into macrosystems ecology of rivers.

Plain Language Summary Rivers can appear different colors such as blues, greens, browns, and yellows. Water color is linked to water quality and can be related to the amount of sediment, algae, and dissolved organic carbon in water. Humans can therefore discern waters' suitability for use with our eyes. While we know many rivers are impaired globally, often due to poor water quality, the color of rivers has not been widely measured to investigate changes through space and time. Satellites act as "eyes in the sky" and regularly observe earth's large rivers. Using satellite remote sensing records from 1984 to 2018, we measured the color of rivers across the USA. We found that large rivers have distinct seasonal patterns in color that change with river flow, and that the dominant color in one third of rivers has significantly changed. Observations of water color can pinpoint rivers undergoing rapid environmental change and work toward continental-scale understanding of rivers.

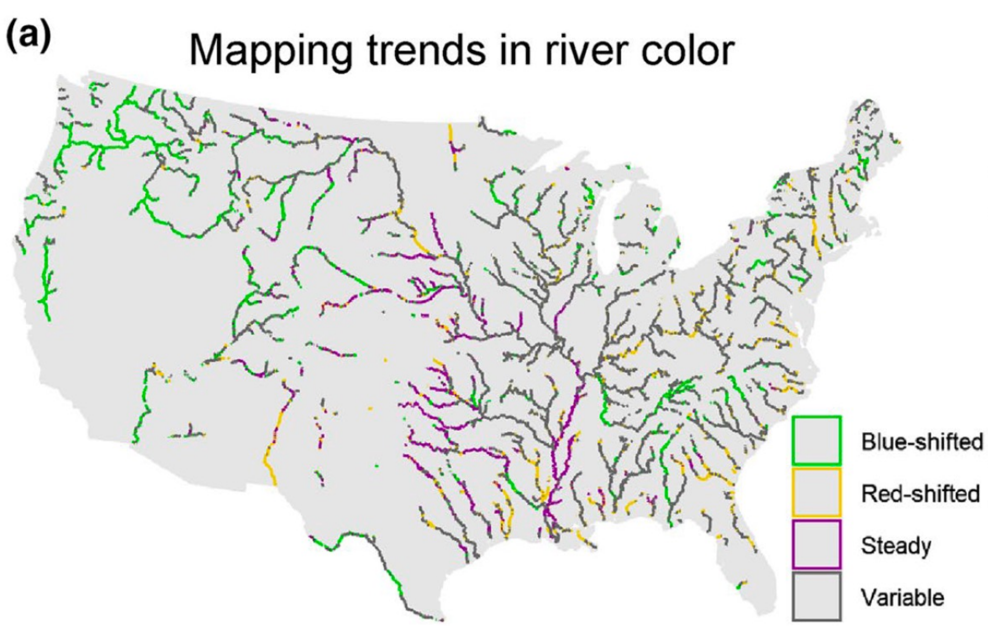

In the east, the reflectance of these rivers shifted to yellowish-red wavelengths, indicating a greater load of suspended sediments. In the west, the reflectance of rivers has shifted to the blue-green end of the spectrum, perhaps as a result of a proliferation of dams that slow the flow of rivers and allow sediments to settle out.

Schlesinger 2021
Translational Ecology
https://blogs.nicholas.duke.edu/citizenscientist/the-source-of-the-yellow-river/

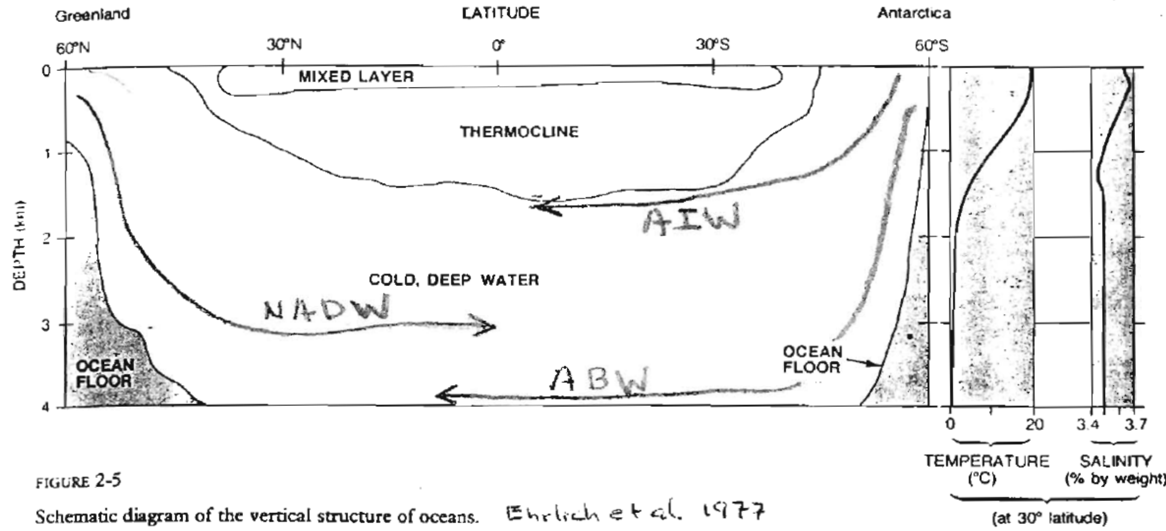

FIGURE 2-5

Schematic diagram of the vertical structure of oceans. Ehrlich et al. 1977

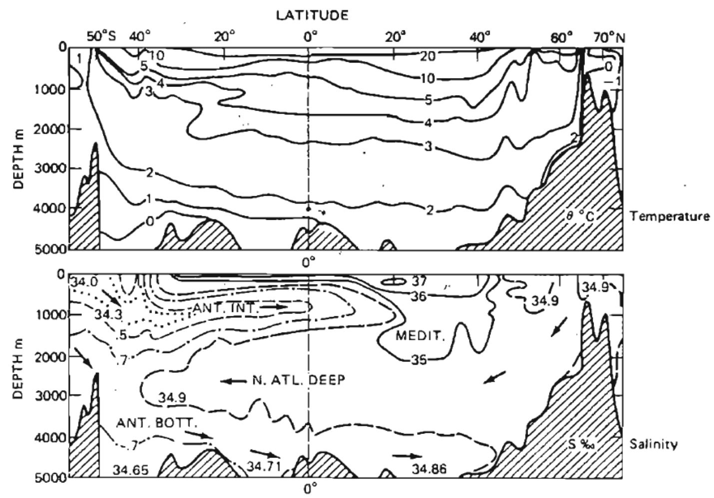

Figure 2.14 South-north vertical sections of water properties of the Atlantic Ocean along the western trough as delineated by lines of constant temperature and salinity. N. Atl. Deep = North Atlantic Deep Water; Ant. Bott. = Antarctic Bottom Water; Ant. Int. = Antarctic Intermediate Water; Medit. = Mediterranean Water. (After Pickard and Emery 1982, based on data from Bainbridge, 1976.)

Berner + Berner 1987

Table 9.1 Major Ion Composition of Seawater, Showing Relationships to Total Salinity and Mean Residence Times for the Elements with Respect to River Water Inputs

Constituent	Concentration in Seawater[a] (mg/kg)	Chlorinity Ratio[a]	Concentration in River Water[b] (mg/kg)	Mean Residence Time (10^6 yr)
Sodium	10,760	0.5561	5.15	75
Magnesium	1294	0.0668	3.35	14
Calcium	412	0.0213	13.4	1.1
Potassium	399	0.0206	1.3	11
Strontium	7.9	0.00041	0.03	12
Chloride	19,350	1.0000	5.75	120
Sulfate	2712	0.1400	8.25	12
Bicarbonate	145	0.0075	52.	0.10
Bromide	67	0.0035	.02	100
Silicate	2.9	0.00015	10.4	0.02
Boron	4.6	0.00024	0.01	10.0
Fluoride	1.3	0.000067	0.10	0.5
Water	35155.7	Σ 1.816667		0.036

[a] Holland (1978).

[b] Meybeck (1979) and Holland (1978).

A CLOSER LOOK

The Salt Content of the Oceans and the Age of Earth

Following ideas first expressed by British astronomer Sir Edmund Halley in 1715, Irish scientist John Joly attempted to calculate the age of Earth on the basis of estimates of the salt content of the ocean and the rate of delivery of salts to the ocean. Two hundred years after Halley, Joly calculated Earth to be 80–89 million years old. However, we now know that Earth is approximately 4.6 billion years old. So where did Joly go wrong?

Joly assumed that the ocean had simply been accumulating all the salts delivered to it by rivers at a constant rate since Earth first formed. Joly neglected the various processes that remove salts from seawater (see the accompanying text). Repeating Joly's calculations but using current estimates of ocean volumes and salinities, we obtain the following:

- The total amount of salt in the oceans is approximately 5×10^{19} kg.
- The rate at which rivers deliver salt is 4×10^{12} kg/yr.
- Therefore, the "age" of Earth is $5 \times 10^{19}/4 \times 10^{12} = 13 \times 10^{6}$ yr.

Thirteen million years is somewhat less than Joly calculated with his knowledge of the world's river discharge, chemical composition, ocean volume, and salt content. The "age" that we have calculated is, in fact, the average length of time salt remains in the ocean. As we will see in Chapter 7, the length of time a substance remains in a given reservoir is called the *residence time*.

Kump et al. 2004

Mechanisms of ion removal from seawater

Na^+ & Cl^-	Pore-water burial Sea-spray salts Sabkhas (salt flats)
Mg^{++}	Hydrothermal exchange
Ca^{++} & $SO_4^{=}$	Biogenic sediments $CaCO_3$ in shells FeS_2 (pyrite) from microbial production of H_2S (hydrogen sulfide) from $SO_4^{=}$
K+	Cation exchange? Clay minerals?

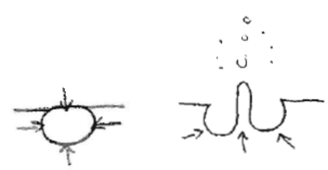

White cliffs of Dover

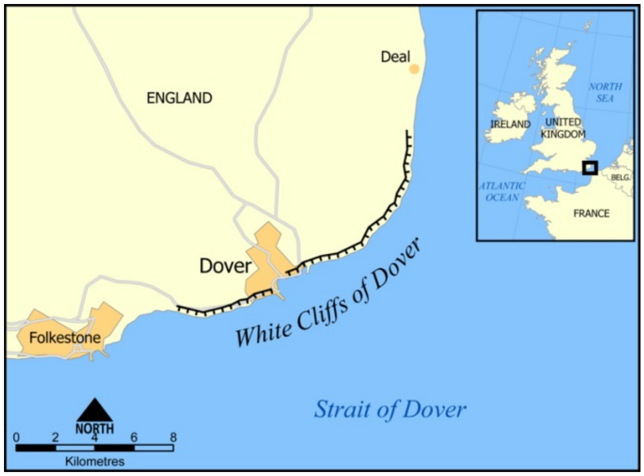

Ocean Circulation

Surface currents

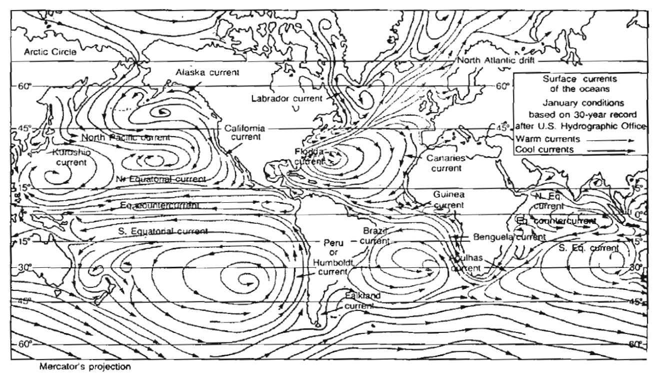

FIGURE 2-6
Main oceanic surface currents. Ehrlich et al. 1977

Deep water circulation

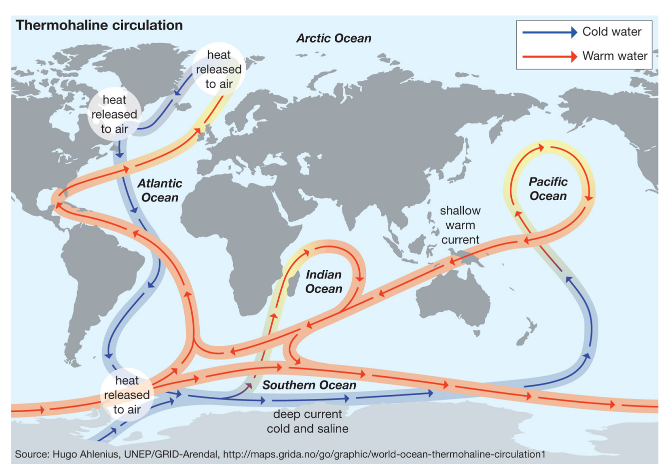

Surface currents

Factors creating ocean gyres

Coriolis Effect

Apparent curvature in the direction of travel of a body moving over a spinning object.

For winds and ocean currents, it's caused by latitudinal differences in the rotational speed of Earth.

Mathematically:

$C = [2\ \Omega \sin(\Phi)]\ V_m$

V_m = Horizontal velocity along meridian

Ω = Rotation rate of Earth (7.3×10^{-5} radians/s)

Φ = Latitude

Ekman Drift

Net transport of surface water 90^o to the right of the wind in the N. Hemisphere and 90^o to the left in the S. Hemisphere.

Latitudinal differences in rotational speed

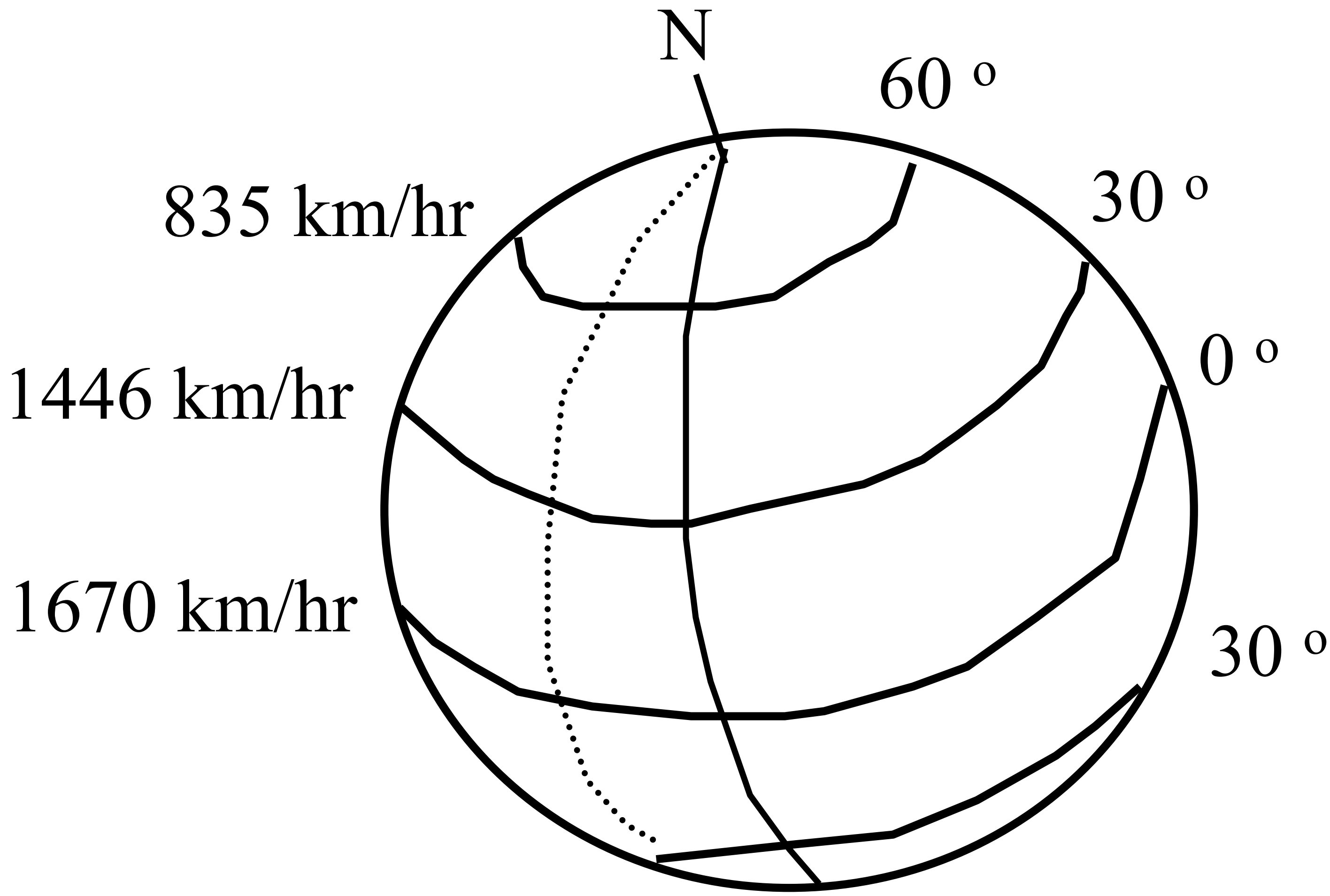

1 km = 0.6214 miles (1038 mph @ Equator)

Earth rotates out from under objects in motion over its surface creating a curved path for observers on the surface.

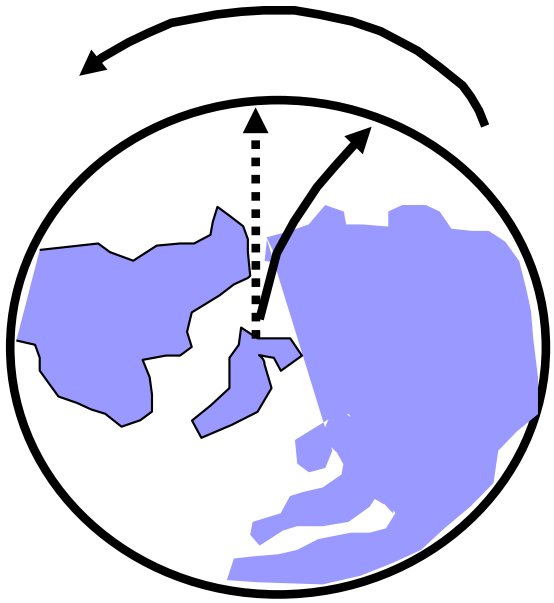

Northern Hemisphere

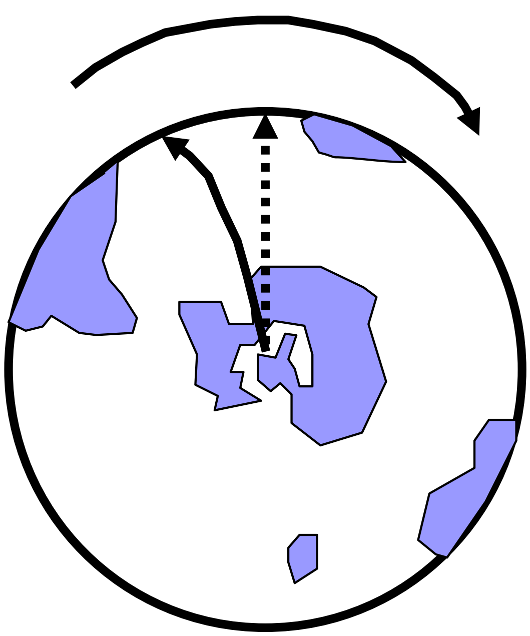

Southern Hemisphere

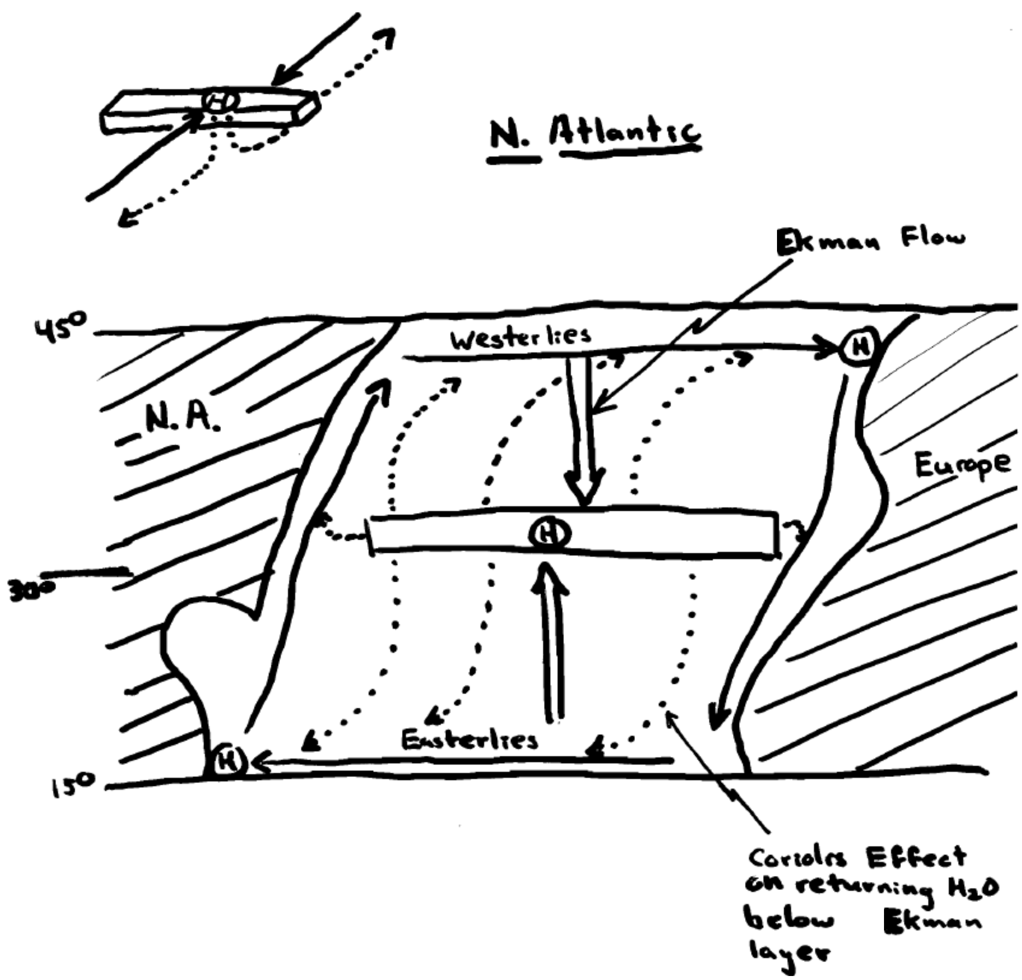

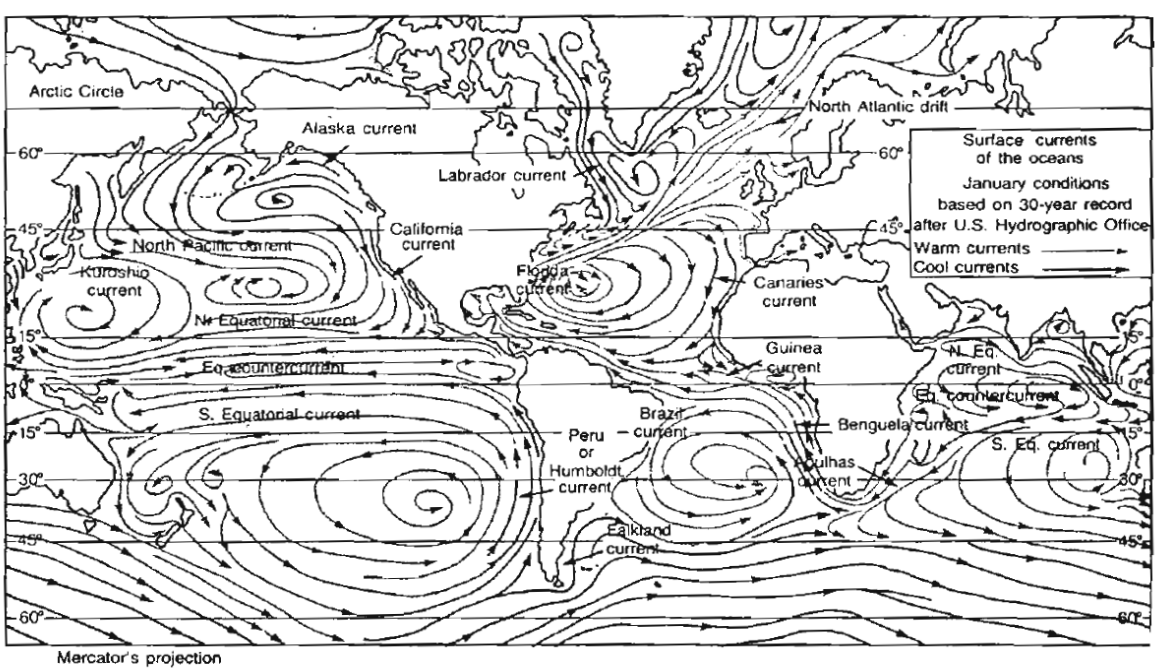

FIGURE 2-6

Main oceanic surface currents. Ehrlich et al. 1977

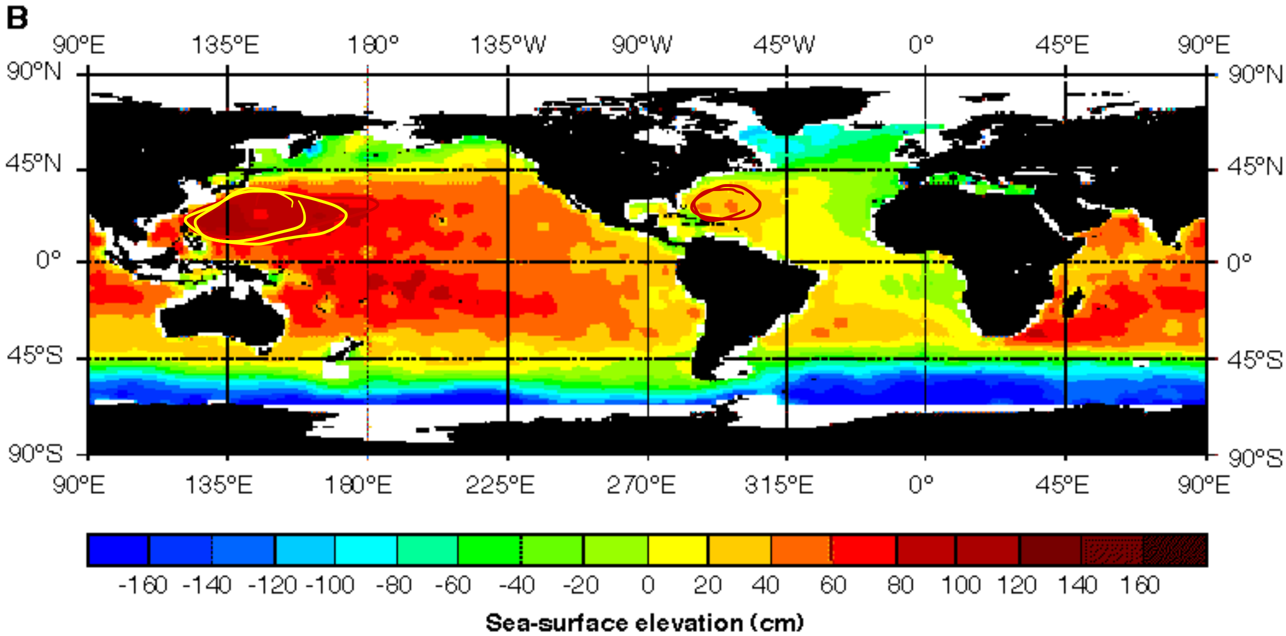
B
90°E
135°E
180°
135°W
90°W
45°W
0°
45°E
90°E
90°N
45°N
0°
45°S
90°S
90°E
135°E
180°E
225°E
270°E
315°E
0°
45°E
90°E
-160 -140 -120 -100 -80 -60 -40 -20 0 20 40 60 80 100 120 140 160
Sea-surface elevation (cm)

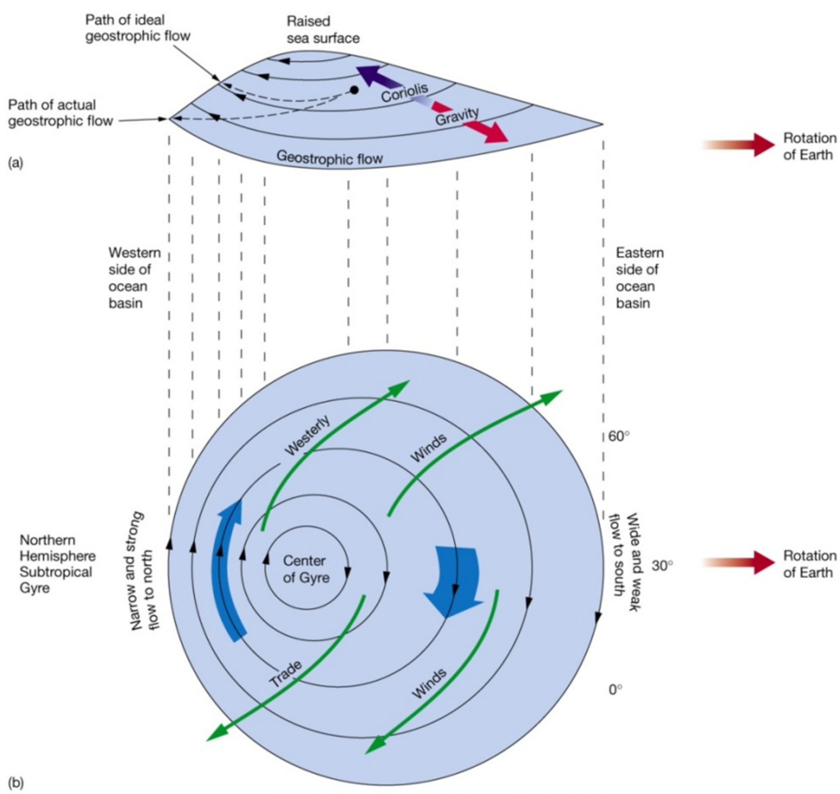
Path of ideal geostrophic flow
Raised sea surface
Path of actual geostrophic flow
Coriolis
Gravity
Geostrophic flow
(a)
Rotation of Earth
Western side of ocean basin
Eastern side of ocean basin
Westerly
Winds
60°
Northern Hemisphere Subtropical Gyre
Narrow and strong flow to north
Center of Gyre
Wide and weak flow to south
30°
Rotation of Earth
Trade
Winds
0°
(b)

Deep water circulation

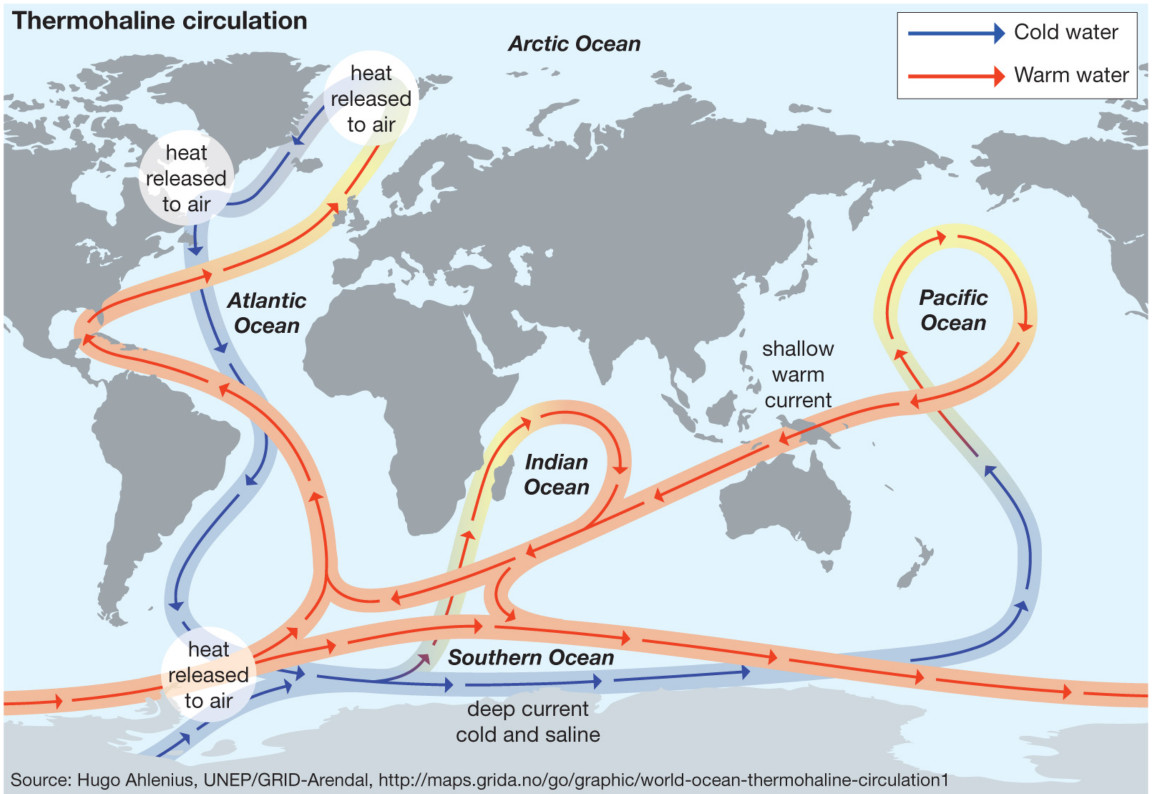

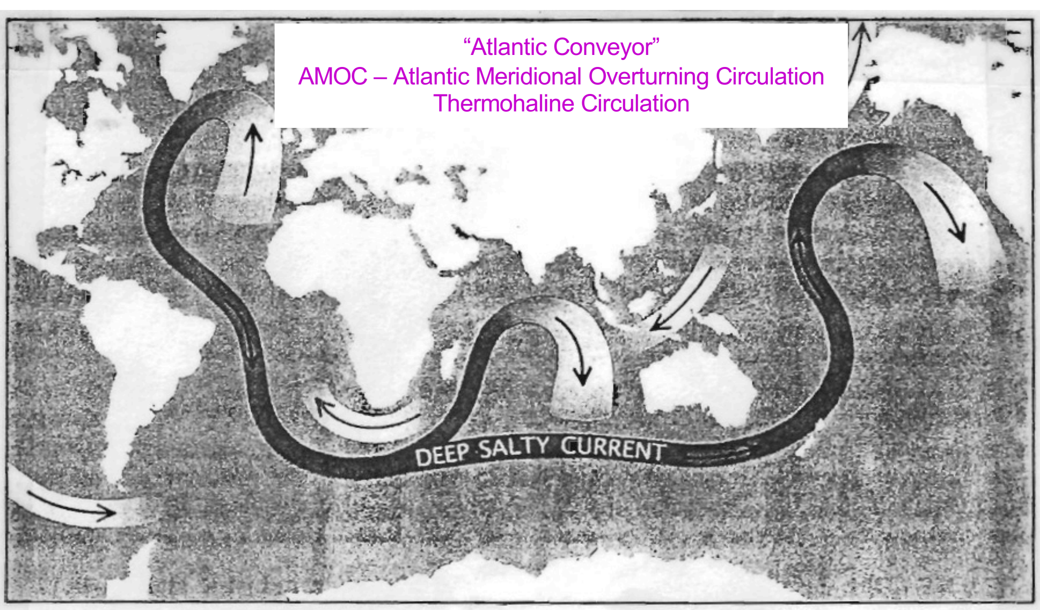

DEEP SALTY CURRENT threads the world's oceans, compensating for the transport of water vapor by the atmosphere. (Light blue arrows indicate shallow return flow.) The current originates in the North Atlantic, where northward-flowing warm water that is unusually saline (and therefore dense) because of excess evaporation is chilled, which increases its density further. It sinks into the abyss and flows southward, out of the Atlantic. Most of the salty water that is supplied by this Atlantic "conveyor" mixes upward in the Pacific, making up for excess precipitation there. The Atlantic conveyor—and probably the entire system—was disrupted during glacial time.

Broecker + Denton 1990

Upwelling & Ekman Drift

Ekman Spiral

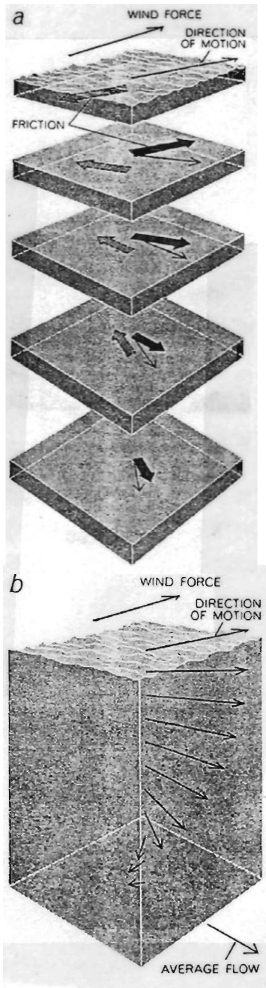

BODY OF WATER can be thought of as a set of slabs (*a*), the top one driven by the wind and each driving the one below it by friction. At each stage the speed of flow is reduced and (in the Northern Hemisphere) directed more to the right. This "Ekman spiral" persists until friction becomes negligible. The "Ekman layer" in which this takes place (*b*) behaves like the frictionless slabs in the preceding illustrations. Its average flow is at right angle to wind driving it.

Stewart 1966

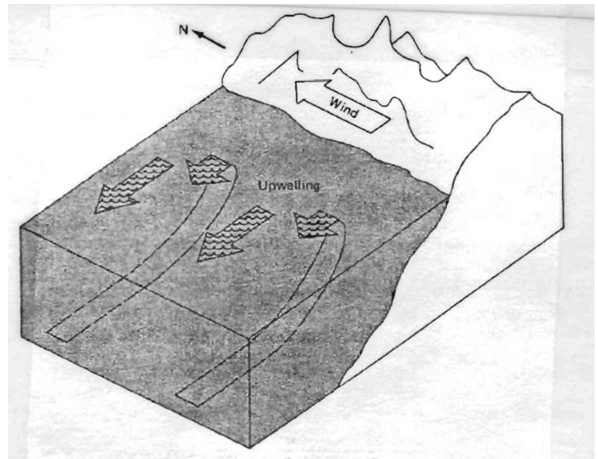

Figure 2.13 Upwelling, or the result of Ekman drift, in response to a north-blowing wind in the Southern Hemisphere. (After K. K. Turekian, *Oceans, 2nd ed.* Copyright © 1976, p. 35. Reprinted by permission of Prentice-Hall, Inc., Englewood Cliffs, N.J.) Berner & Berner 1987

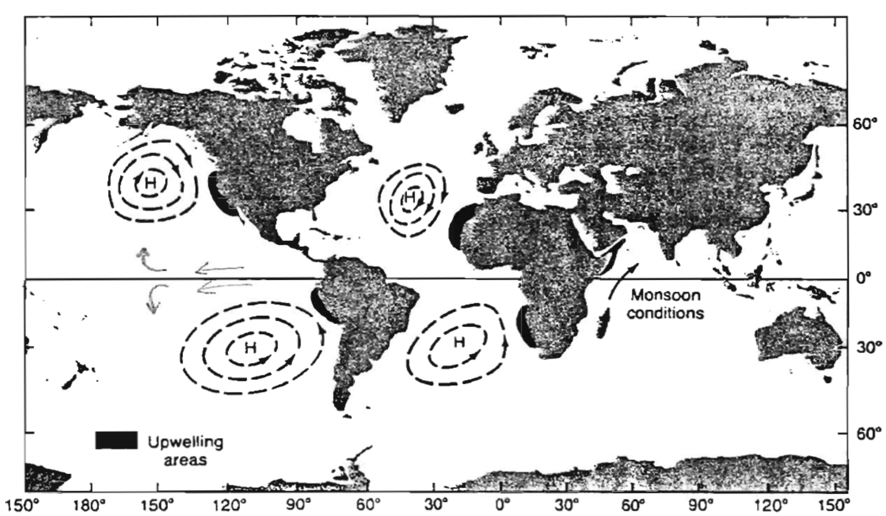

FIGURE 9-16 The major coastal upwelling areas of the world (shaded) and the weather circulation patterns that drive them. (Adapted from Hartline, 1980.)
Ross 1982

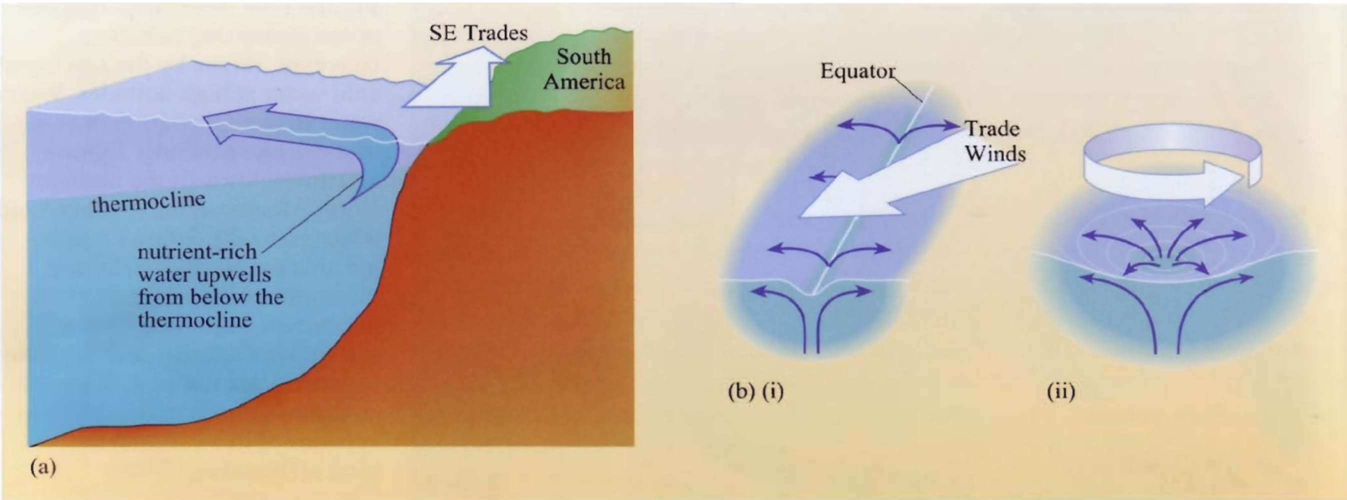

Figure 1.36 (a) Equatorwards winds along the coast of Peru and Chile lead to offshore current flow (i.e. to the left of the wind, as this is in the Southern Hemisphere), causing divergence of water from the coast and upwelling of nutrient-rich water from below the thermocline. (b) Schematic diagrams to show other types of wind fields that lead to upwelling: (i) Trade Winds crossing the Equator (where the Coriolis force is zero) lead to a zone of upwelling along the Equatorial Divergence. (ii) Cyclonic winds lead to divergence of surface water and mid-ocean upwelling (here shown for the Northern Hemisphere); by contrast, anticyclonic winds lead to convergence of surface water and downwelling.

Cockell et al. 2007

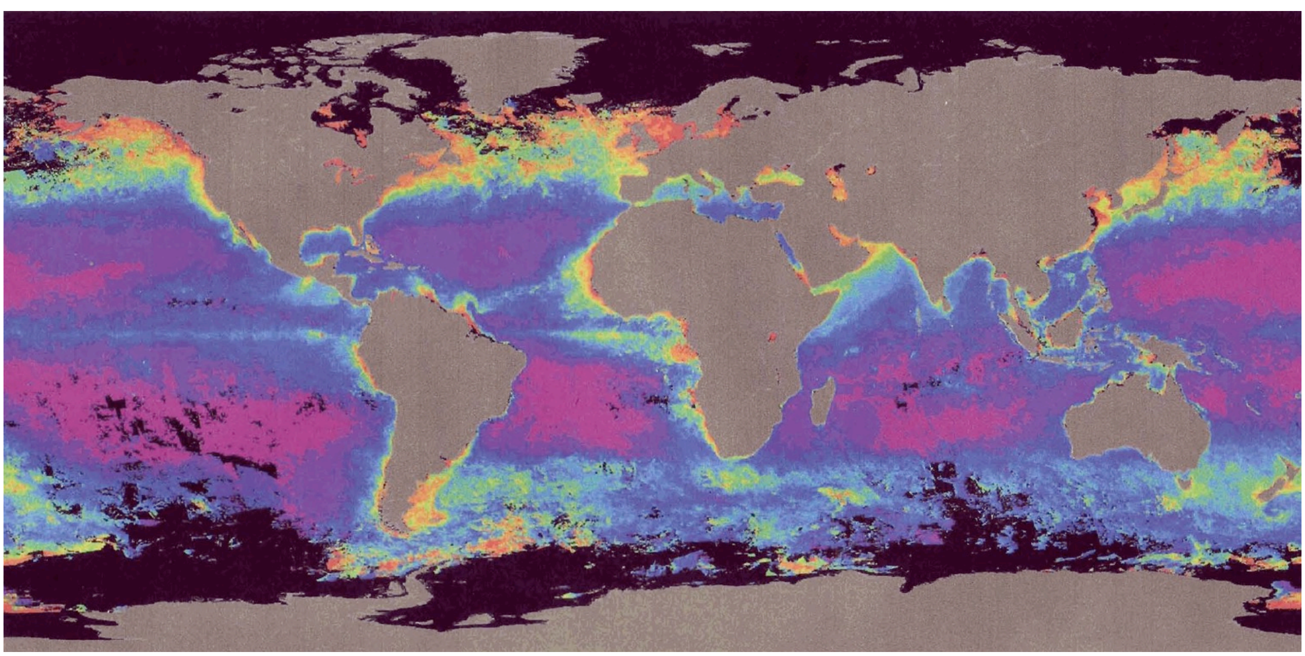

nature climate change

ARTICLES
PUBLISHED ONLINE: 23 MARCH 2015 | DOI: 10.1038/NCLIMATE2554

Exceptional twentieth-century slowdown in Atlantic Ocean overturning circulation

Stefan Rahmstorf[1*], Jason E. Box[2], Georg Feulner[1], Michael E. Mann[3,4], Alexander Robinson[1,5,6], Scott Rutherford[7] and Erik J. Schaffernicht[1]

Possible changes in Atlantic meridional overturning circulation (AMOC) provide a key source of uncertainty regarding future climate change. Maps of temperature trends over the twentieth century show a conspicuous region of cooling in the northern Atlantic. Here we present multiple lines of evidence suggesting that this cooling may be due to a reduction in the AMOC over the twentieth century and particularly after 1970. Since 1990 the AMOC seems to have partly recovered. This time evolution is consistently suggested by an AMOC index based on sea surface temperatures, by the hemispheric temperature difference, by coral-based proxies and by oceanic measurements. We discuss a possible contribution of the melting of the Greenland Ice Sheet to the slowdown. Using a multi-proxy temperature reconstruction for the AMOC index suggests that the AMOC weakness after 1975 is an unprecedented event in the past millennium ($p > 0.99$). Further melting of Greenland in the coming decades could contribute to further weakening of the AMOC.

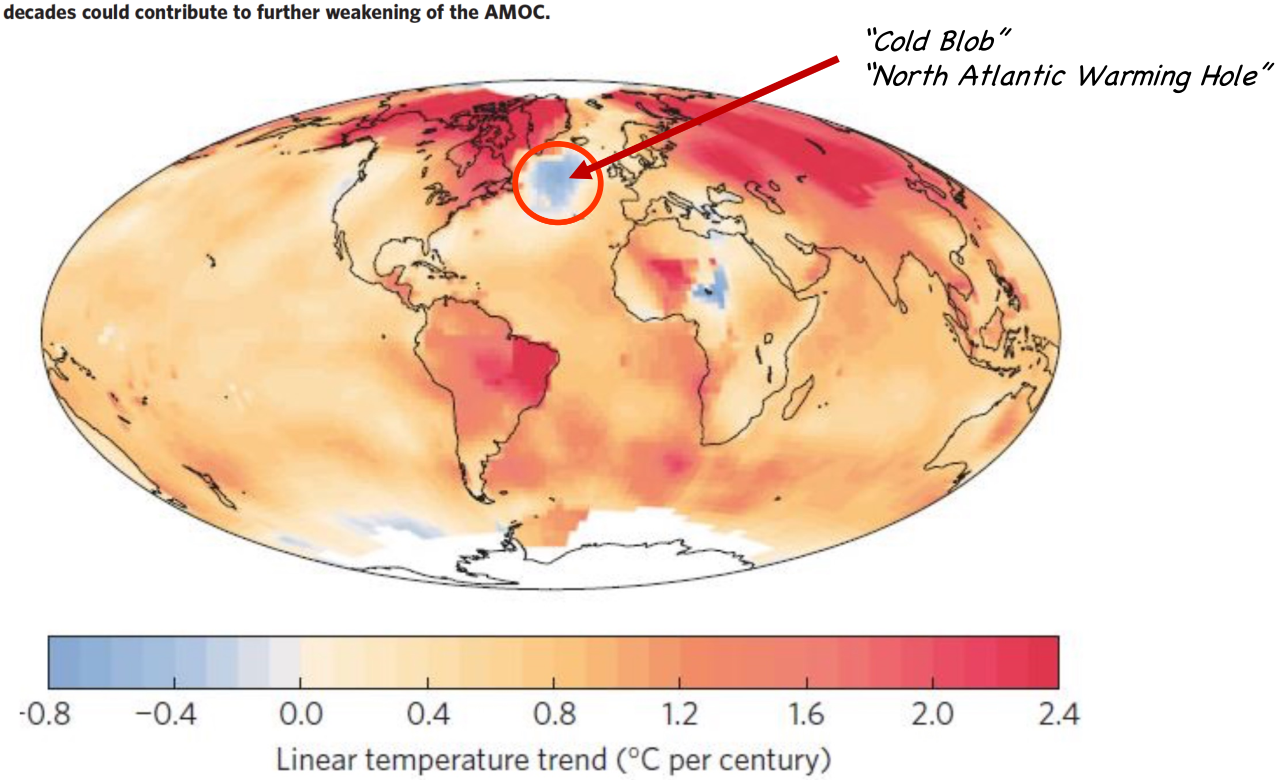

***Fig. 1** Linear temperature trend from 1900 to 2013. The cooling in the subpolar North Atlantic is remarkable and well documented by numerous measurements – unlike the cold spot in central Africa, which on closer inspection apparently is an artifact of incomplete and inhomogeneous weather station data.*

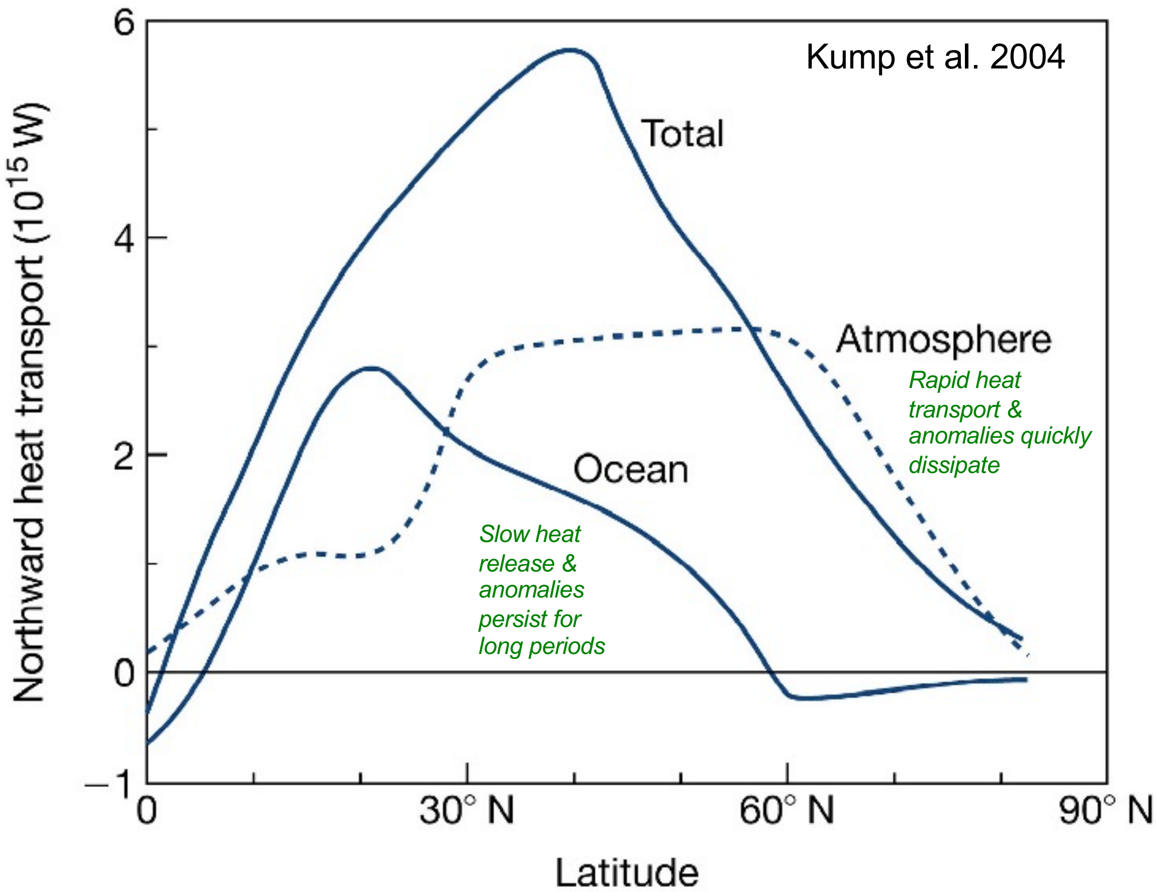

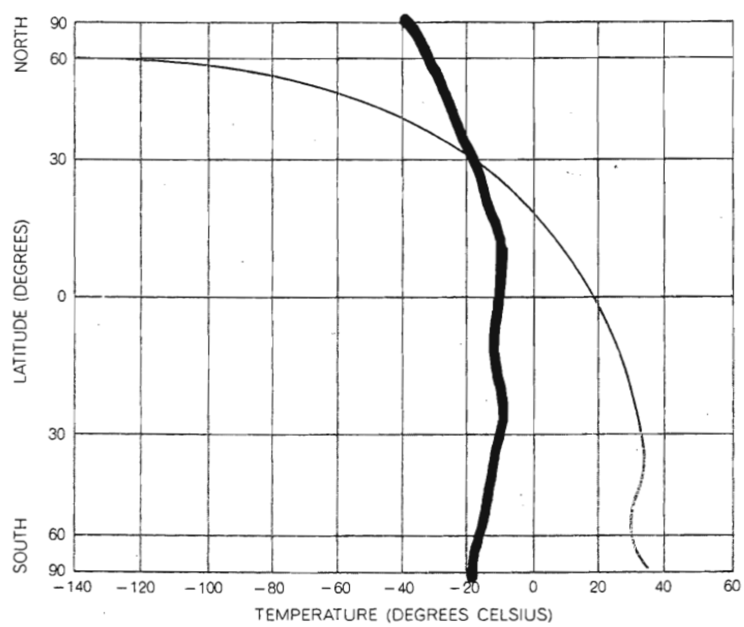

IMPORTANCE OF ATMOSPHERIC DYNAMICS in moderating the earth's climate is demonstrated by this graph, which compares the calculated radiative-equilibrium temperature for a "black" earth (*colored curve*) with the observed vertical mean temperature (*black curve*) as a function of latitude during January. At this time no sunshine reaches the earth north of the Arctic Circle; neglecting any lag effects due to the storage of heat, the radiative-equilibrium temperature in the polar cap would go down to absolute zero (−273.2

Oort 1970